Journal of Applied Geophysics 208 (2023) 104888

Contents lists available at ScienceDirect

Journal of Applied Geophysics

journal homepage: www.elsevier.com/locate/jappgeo

The sensitivity of seismic refraction velocity models to survey geometry errors, assessed using Monte Carlo analysis

Hannah Watts [a,b,*], Adam D. Booth [c], Roger A. Clark [c], Benedict T.I. Reinardy [b,d]

[a] Stockholm University, Department of Physical Geography, Stockholm, Sweden
[b] Bolin Centre for Climate Research, Stockholm, Sweden
[c] University of Leeds, School of Earth and Environment, Leeds, UK
[d] KTH Royal Institute of Technology, School of Architecture and the Built Environment, Stockholm, Sweden

ARTICLE INFO

Keywords:
Seismic refraction
Plus-Minus
Monte Carlo
Uncertainty
Near-surface geophysics

ABSTRACT

Seismic refraction models should routinely be reported with their associated uncertainty. Tomographic solutions are widespread, but estimating uncertainties in these via Monte Carlo simulation places great demands on computer resource, hence this task is often omitted. By considering the Plus-Minus method of seismic refraction interpretation, we use Monte Carlo simulations to evaluate the uncertainty in seismic refraction results and determine the sources of uncertainty that are most impactful on the reliability of the output model. Our analysis considers the impact of survey mislocation (i.e., geophones misplaced from a planned position) and interpretational problems (i.e., misidentification of first-break picks and uncertainty in identifying crossover distances) on the overall uncertainty in inferred unit thicknesses and seismic velocities. These are considered for synthetic data with varying subsurface velocity structure, and for field data collected at a shallow (< 50 m) bedrock site in north Wales (UK). Analysis of synthetic data shows that the impact of the aforementioned errors on thickness estimates is ~1000 times that on velocity estimates. Of all permutations tested, the most significant impact on thickness uncertainty was the accuracy of first-break picks, with the variance in target thickness estimates increasing roughly exponentially with first-break pick uncertainty. It is therefore prudent to minimise such uncertainty through appropriate survey practice (e.g., maximising source energy, taking multiple shots for stacking) and to properly define the resultant uncertainty in unit thickness and velocity estimates. The simplicity of the Plus-Minus method makes it an effective tool for highlighting the errors that would impact more sophisticated interpretation approaches, such as tomography or Full Waveform Inversion. The results from such analysis can be directly applied in straightforward environmental or engineering investigations and can be used to inform more advanced refraction methods. As such, the practice we highlight should be considered for any refraction interpretation.

1. Introduction

Depths and physical properties provided by geophysical methods should be routinely reported with their associated uncertainties (Beven, 2018). Results quoted without such information may be applied with undue confidence and lead to misrepresentative interpretations. Seismic refraction (hereafter referred to as refraction) techniques are commonly used in geotechnical and environmental site investigations (e.g., Mollaret et al., 2020; Pegah and Liu, 2016; Rossi et al., 2018) to determine seismic velocity-depth profiles using the first-arrival times of seismic energy at a series of receivers, after deploying a seismic source (Berry, 1971). There are numerous methods of interpreting refraction data, including intercept-time techniques (Ewing et al., 1939), reciprocal methods (e.g., Hagedoorn, 1959; Hawkins, 1961; Palmer, 1981), wavefront reconstruction methods (Rockwell et al., 1967), travel-time tomography (e.g., Schuster and Quintus-Bosz, 1993), and full waveform inversions (Tarantola, 1986; Virieux and Operto, 2009). These provide estimates of subsurface velocity structure, honouring different levels of complexity while applying various simplifying assumptions. Due to inevitable uncertainties in the refraction interpretation inputs, the output models of velocity and depth are inherently uncertain. Therefore, it is crucial that refraction results are always reported with their associated uncertainty (Dampney and Whiteley, 1980). Traditional methods used to calculate this output uncertainty involve evaluating the

* Corresponding author at: Stockholms universitet, Institutionen för naturgeografi, 106 91 Stockholm, Sweden.
E-mail address: Hannah.watts@natgeo.su.se (H. Watts).

https://doi.org/10.1016/j.jappgeo.2022.104888
Received 20 July 2022; Received in revised form 30 September 2022; Accepted 20 November 2022
Available online 24 November 2022

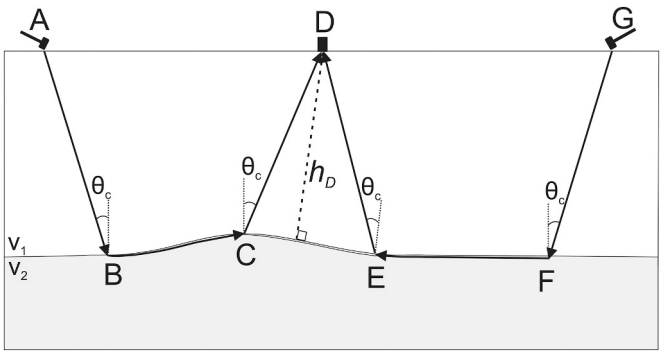

Fig. 1. The ray paths and lettering conventions used in the Plus-Minus method calculations.

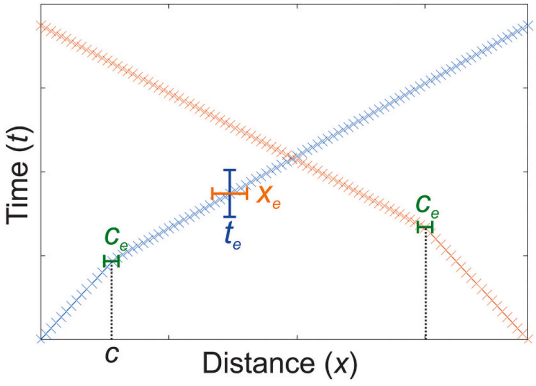

Fig. 2. Example time-distance plot (arrivals from shotpoint A and G displayed in blue and orange, respectively; Fig. 1) illustrating the errors considered in this analysis: first-break pick time (t_e), shot-geophone offset (x_e), and cross-over distance (c_e). (For interpretation of the references to colour in this figure legend, the reader is referred to the web version of this article.)

error in least-square straight-line fitting (e.g., Booth et al., 2013; York et al., 2004), which only gives an average depth error for the refractor, or they involve manually recalculating the refraction outputs using extreme input values, which is laborious and does not necessarily produce the maximum possible output uncertainties (Northwood, 1967). Recently, methods have been developed to define the uncertainty in the outcomes of tomographic inversion (Egorov et al., 2022; Ryberg and Haberland, 2018), but the large number of degrees of freedom in these imposes significant computational demands hence they are seldom implemented in environmental or engineering investigations.

Monte Carlo (MC) simulations are an effective means to propagate uncertainties from refraction inputs to the output results (Anderson, 1976; Cox and Siebert, 2006). They incorporate input error distributions allowing flexible representation of plausible uncertainty scenarios. Hagedoorn's (1959) Plus-Minus method (PM) for refraction interpretation is valued for its ability to delineate undulating refractors with relatively few straightforward equations, provided the subsurface velocity structure is relatively simple (van Overmeeren, 2001). This means error analysis can be easily performed without the computational burden required for Monte Carlo tomographic simulations (Huang et al., 2021; Ryberg and Haberland, 2018). Applying MC to PM calculations efficiently provides probability density functions (pdfs) for unit thicknesses beneath each geophone location (h_D) and unit p-wave velocities (v_p). These results can provide constraints for starting models when undertaking inversions, such as refraction tomography or multichannel analysis of surface waves (MASW). This minimises the uncertainty that is introduced by the model applied during the inversion process, to produce accurate inversion outcomes. Northwood (1967) noted that first-break time pick accuracy is a significant factor in refractor depth uncertainty but quantitative evaluation of its effect was limited by the need to repeat the whole interpretation multiple times. MC simulations overcome this issue and are well suited to sensitivity analysis, allowing quantification of how individual input errors affect the uncertainty of the results.

In this paper, we review the PM method, MC simulations, and sensitivity analysis, and apply them to a range of synthetic data scenarios to show how varied survey errors combine to influence the uncertainty in the interpretation for various layered velocity models. We then apply the method using a seismic dataset from North Wales (UK). We illustrate the impact of different surface conditions and data quality on the uncertainty in the refractor depths and highlight the implications of this analysis for survey procedure. These analyses demonstrate that, for most plausible velocity models, the greatest survey effort should be placed on ensuring that first-break travel-times can be picked with minimum ambiguity.

Table 1
Model parameters used to create synthetic t-x pairs for sensitivity analysis. gx is an abbreviation of geophone. Za and Zb are the refractor depths at either end of the profile, with a linear slope between.

2-layer	V_1 (m/s)	V_2 (m/s)	Za (m)	Zb (m)	Geophone spacing (m)	No. of geophones	Spread length (m)
Baseline	1500	3000	8	12	2	96	190
Shallow	1500	3000	4	8	2	96	190
Deep	1500	3000	12	16	2	96	190
High V	3000	5500	8	12	2	96	190
Low V	150	2650	8	12	2	96	190
High contrast	500	5850	8	12	2	96	190
Low V, high contrast	150	5500	8	12	2	96	190
Low contrast	500	750	8	12	2	96	190
Small gx intervals	1500	3000	8	12	1	192	191
Large gx intervals	1500	3000	8	12	4	48	188
Short spread	1500	3000	8	12	2	48	94
Long spread	1500	3000	8	12	2	192	382

3-layer	V1 (m/s)	V2 (m/s)	V3 (m/s)	Z1 (m)	Z2a (m)	Z2b (m)	Geophone spacing (m)	No. of geophones	Spread length (m)
High velocity	500	2750	5000	3	8	12	2	96	190
Low velocity	150	500	3000	3	8	12	2	96	190
High contrast	150	500	5850	3	8	12	2	96	190
Low contrast	150	1000	3250	3	8	12	2	96	190

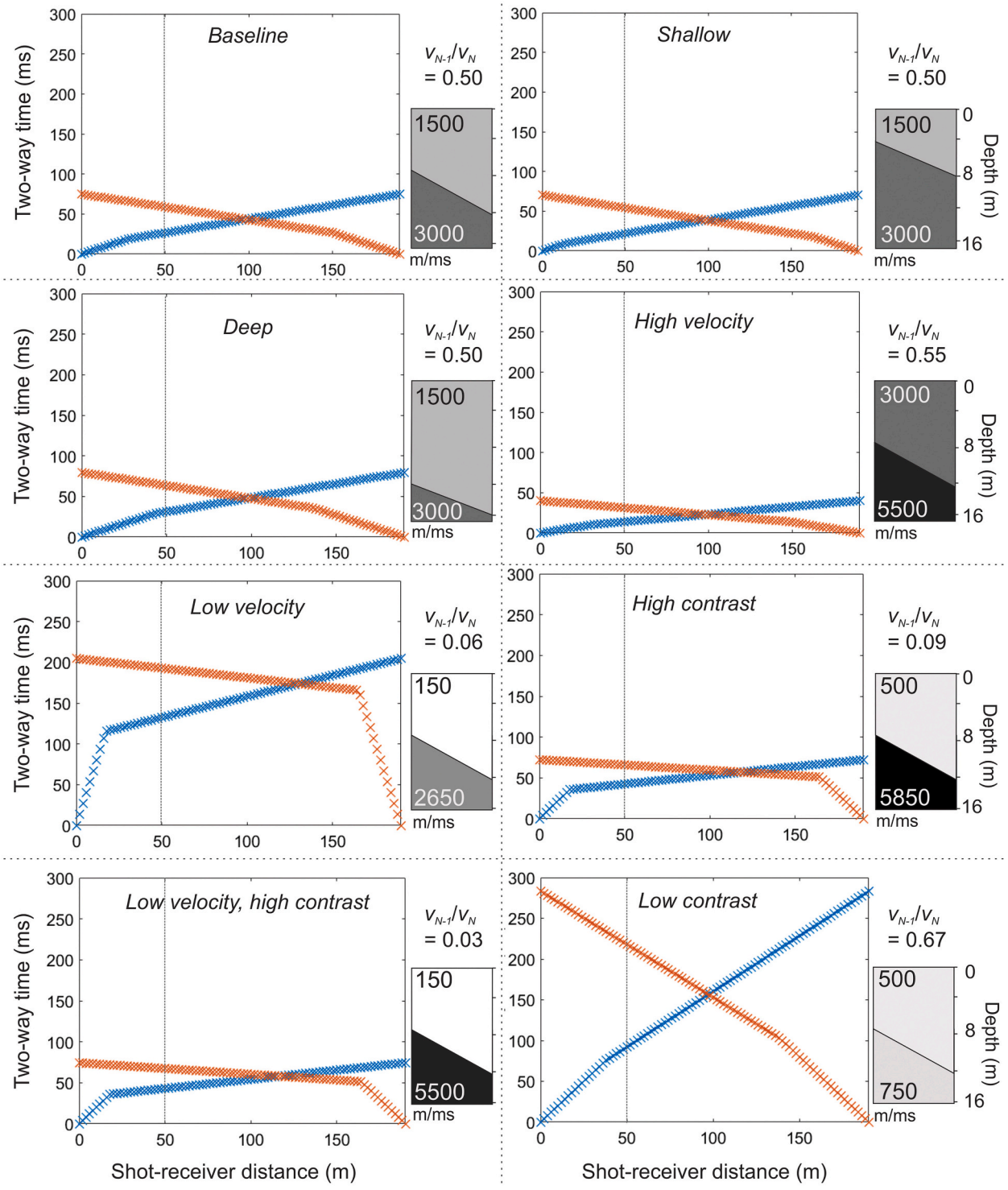

Fig. 3. Time-distance plots for the synthetic models used in this analysis. Model names correspond to Table 1. Arrivals from shotpoints A and G (Fig. 1) are displayed in blue and orange, respectively. Dotted vertical lines mark the location of the geophone offset 50 m from shotpoint A, used in error analysis. To the right of each time-distance plot, the velocity ratio between the target unit (N) and the overlying unit (N-1) is displayed along with a schematic of the model used to create the synthetic data; darker colours indicate higher velocities. (For interpretation of the references to colour in this figure legend, the reader is referred to the web version of this article.)

1.1. Hagedoorn's Plus-Minus interpretation method

PM was developed by Hagedoorn (1959) to enable efficient yet reasonable approximations of unit boundary depths and seismic wave velocities from refraction data when surface topography is minimal and a laterally homogeneous, layered subsurface is present. PM is based on the wavefront method of Thornburgh (1930) and the Delay-Time concept of Gardner (1939, 1967), and was subsequently developed into the reciprocal method (Hawkins, 1961). Algorithms have since been established to improve the representation of refractor geometries, such

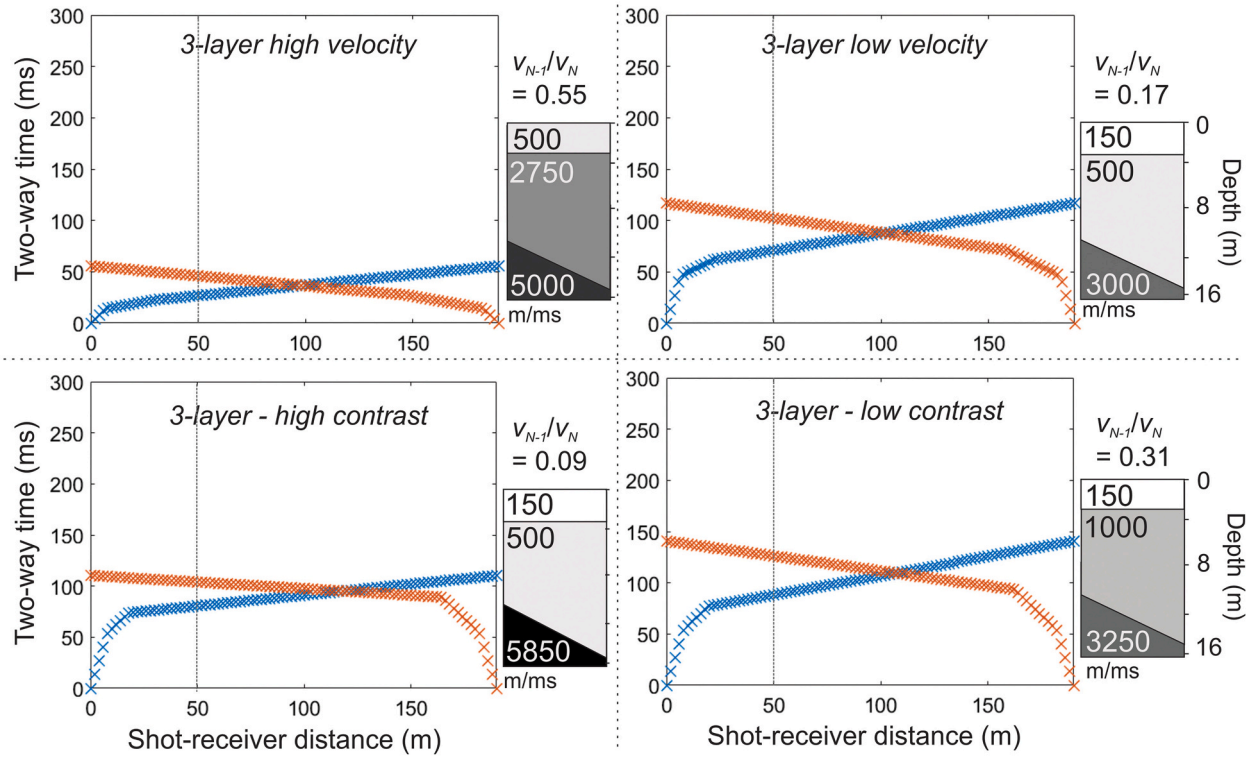

Fig. 3. (*continued*).

Table 2
Error bounds applied to define the Gaussian probability distributions for each execution of the MC process. All five rows were applied to each model. For the 3-layer models, both crossover locations had the same error (c_e). First-break pick errors (t_e) increase linearly from near to far offset geophones.

	x_e (m)	t_e (ms)	c_e
None	0	0	0
Geophone offset	1	0	0
First-break pick	0	0.25–1	0
Crossover distance	0	0	1
All	1	0.25–1	1

as Palmer's (1980) Generalised Reciprocal Method, Visual Interactive Raytracing (Whiteley, 2004), Full Waveform Inversion (Tarantola, 1986), and Wavepath Eikonal Traveltime Tomography (Schuster and Quintus-Bosz, 1993), but these are computationally expensive compared to PM. The simplicity of PM has led to its continued use in near-surface investigations (e.g., Hausmann et al., 2007; Ross et al., 2019), to determine static corrections for seismic reflection investigations (e.g., Bridle, 2007; Opara et al., 2018) and to constrain starting models in seismic inversions (e.g., MASW) (Liu and Stock, 1993). Furthermore, it provides a simple analytic framework for establishing and appreciating the sensitivity of errors to subsurface parameters and survey design.

Data acquisition for PM requires a pair of seismic shotpoints, one situated at each end of a linear geophone array to provide 'forward' and 'reverse' coverage. Interpretation can be applied to the set of geophones where first arrivals from the forward and reverse shots are the critically refracted waves from the target refractor (range of 'reverse cover'; B—F, Fig. 1). Within this range, the unit thickness beneath each geophone, h_D, is determined using the simple calculation of 'Plus Times' (T^+),

$$T^+_D = T_{ABCD} + T_{GFED} - T_{ABFG}, \tag{1}$$

where the T terms are travel-times, defined in Fig. 1. In a two-layer case, h_D is given by:

$$T^+_D = 2(h_D cos\theta_c)/v_1, \tag{2}$$

where v_1 is the seismic velocity in the overburden, calculated from the reciprocal of the slope of the direct wave arrivals on the time-offset (t-x) plot, and $\theta_c = \sin^{-1}(v_1/v_N)$. v_N is the seismic velocity in the target unit and is calculated using 'Minus Times' (T^-),

$$T^-_D = T_{ABCD} - T_{GFED} - T_{ABFG}. \tag{3}$$

v_N is the inverse slope of the graph of T^- against $2x$, where x is shotpoint-geophone offset:

$$\Delta T^- = \frac{2\Delta x}{v_N}. \tag{4}$$

For cases where the target refractor is overlain by multiple layers, overburden layer velocities (i.e., v_i, the velocity in the ith layer from the ground surface) are defined using the inverse slope of the corresponding segments of the t-x plot, v_N is given by eq. (4) and eq. (2) is updated so that the unit thickness for the ith layer, at geophone D (h_{iD}) is given by:

$$T^+_D = \sum_{i=1}^{i=N-1} \frac{2h_{iD}cos\theta_{i,N}}{v_i}, \tag{5}$$

where N is the number of layers. The target refractor depth (z_D) is the sum of the unit thicknesses at geophone D.

The calculation of unit thicknesses and velocities with PM assumes i) homogeneous and isotropic velocities in overburden layers, ii) that the target refractor has a dip angle $<10^o$, and iii) first arrivals are the direct wave or critical refractions (Hagedoorn, 1959; Reynolds, 2011). The issues arising when these assumptions are violated have been investigated by Dampney and Whiteley (1980) and Liu and Stock (1993): deviations from assumption (i) can be detected by repeating refraction calculations for adjacent, overlapping seismic spreads, and the contribution of these deviations to the total result uncertainty can be quantified using MC and the Gibbs sampler (Casella and George, 1992). Assumption (ii) is an improvement on the delay-time method's

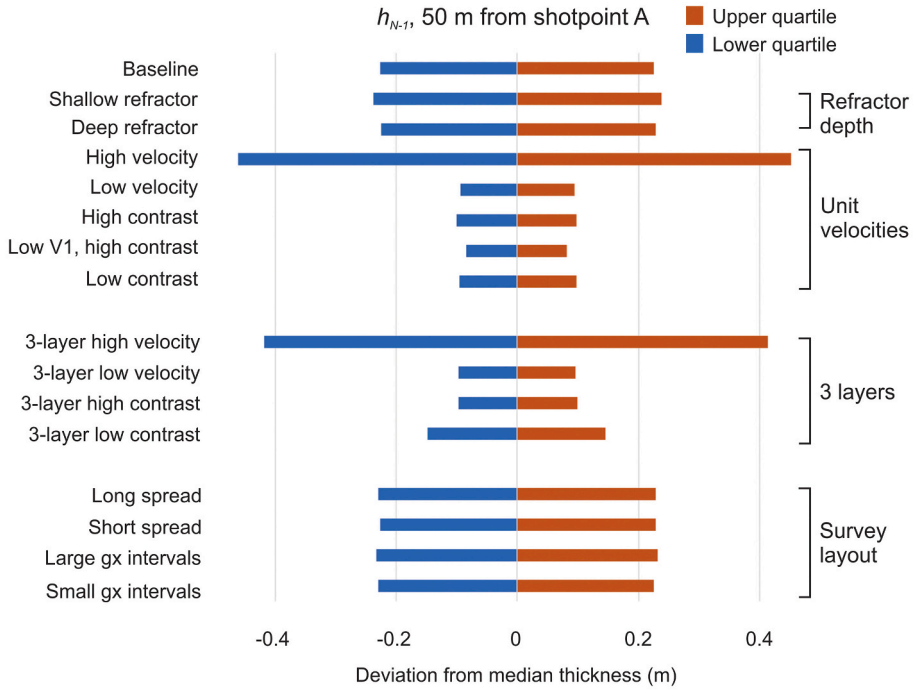

Fig. 4. A plot of the inter-quartile ranges of output h_{N-1} values from Monte Carlo simulations with 'All' errors applied (Table 2) for each of the synthetic datasets, where h_{N-1} is the thickness of the layer above the target refractor 50 m from shotpoint A. Values are normalised around the median output for each model. Labels to the right of the graph state the model variables being explored. The model names correspond to those in Table 2 and Fig. 3. gx is an abbreviation of geophone.

assumption of horizontal refractors (Whiteley and Eccleston, 2006) and while assumptions (ii) and (iii) are rarely met, they are good approximations (Dampney and Whiteley, 1980).

Given the recursive nature of velocities in this system of equations, the cumulative error and uncertainty in the output models increases with subsurface complexity. The uncertainties that we consider are (i) the timings of first-break picks, t_e; (ii) the shot-receiver distances, x_e; (iii) the crossover distances, c_e (i.e., the geophone position at which critically refracted arrivals from one layer are overtaken, and thus identified, by the arrivals from the layer below) (Fig. 2; Dampney and Whiteley, 1980; Northwood, 1967).

The effect of these uncertainties on refraction results has implications for the uncertainty in further analysis, such as the assessment of material properties (e.g., Pegah and Liu, 2020) or the determination of static corrections. Material properties include elastic parameters such as Young's modulus (E) or Poisson's ratio (ν), which are used to determine soil conditions (e.g., strength or resistance to deformation) to ensure they are suitable for a desired construction. Static corrections are applied during seismic reflection investigations to account for (i) the low velocity near surface superficial or weathered layer(s) (the 'weathering correction'), and (ii) surface topography (the 'elevation correction'). They are implemented by applying time shifts to each seismic trace in the reflection acquisition to map source and receiver positions onto a common datum (Yilmaz, 2001), with uniform near-surface velocity v_e (the 'replacement', or 'elevation' velocity). The weathering correction is often computed by using refraction methods, such as PM, to calculate the time in the weathering layer and hence the required shift in travel time (T_w) for each surface location (e.g., Zhu et al., 2014). Therefore, through defining the uncertainty in PM outputs, the uncertainty in T_w can be quantified.

1.2. Error propagation using Monte Carlo simulation

MC simulation is a means of evaluating the distribution of uncertainty in an output model based on the error distributions of the input parameters. The simulations produce m permutations of a given model, using pseudorandom selections of input values from their defined error distributions (e.g., Cox and Siebert, 2006; Hammersley and Handscomb, 1964; Morgan and Henrion, 1990). For a result to be representative, m should exceed $10000/(1-p)$, where p is the percentage of times that an output model falls within a chosen tolerance of the true value (Couto et al., 2013). This process produces output pdfs from which standard statistical values (e.g., mode, variance and percentiles), as appropriate to the character of the pdf, are easily defined (Morgan and Henrion, 1990).

1.3. Sensitivity analysis

The MC approach can be used to assess the sensitivity of the output model to variations in the input variables (Ye and Hill, 2017). For each input, a sensitivity coefficient S_i indicates its contribution to the overall observed uncertainty and, from a practical viewpoint, how much attention should be given to improving it (Hamby, 1994; Razavi and Gupta, 2015). S_i is determined using a global Sobol' method (Sobol", 1993), in which all input variables are varied within their parameter ranges to observe how output uncertainty is affected by changes in the variables and their interactions (Saltelli et al., 2004; Ye and Hill, 2017). The Sobol' method ranks input variables based on their contribution to the output variance, defined using two values: first-order and total-effect sensitivity coefficients. First-order S_i values are calculated for each uncertain input (X_i) using:

$$S_i = \frac{V(X_i)}{V(Y)}, \tag{6}$$

where $V(X_i)$ is the partial variance due to X_i and $V(Y)$ is the total output variance (Sobol", 1993). Total-effect S_i considers interactions between variables, but is not required if there is negligible covariance, $|r|$, between individual X_i and if the purpose of the sensitivity analysis is purely to investigate input error importance (Zhang et al., 2015). In this paper, all further instances of S_i denote first-order S_i.

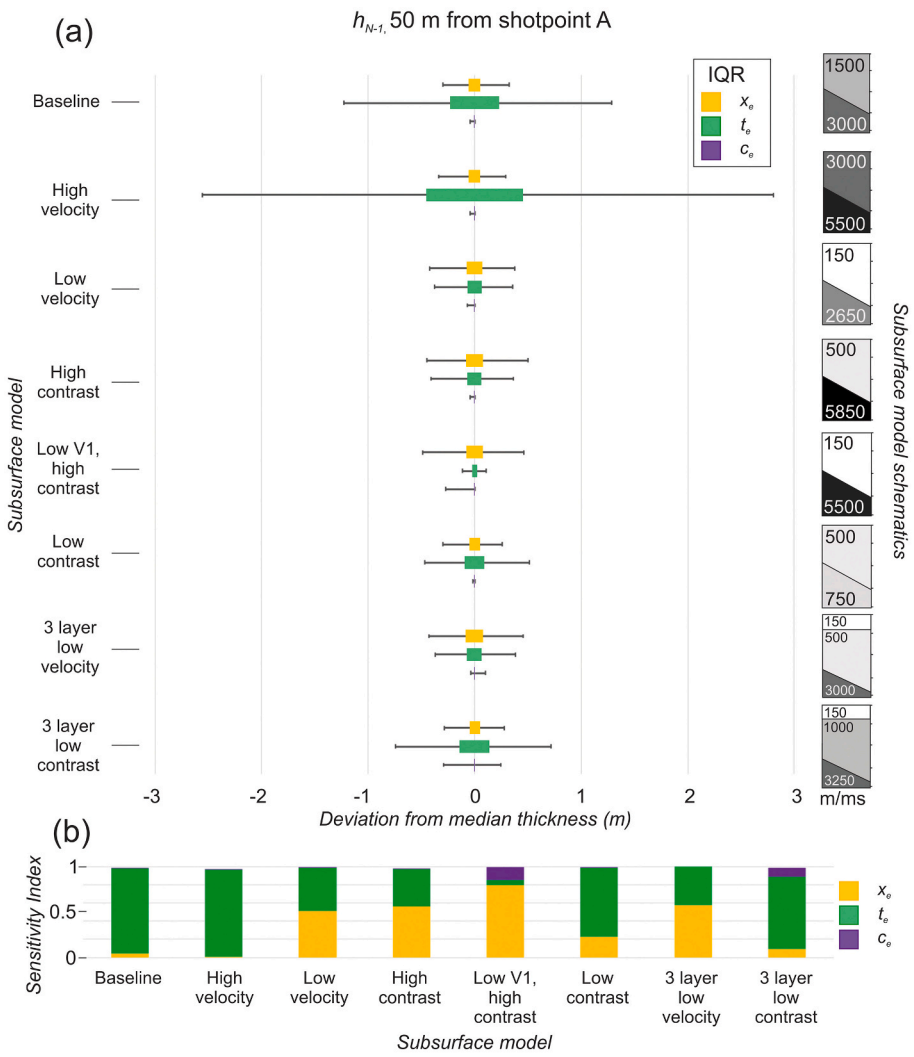

Fig. 5. A breakdown of the contributions of errors in geophone offset (xe), first-break pick time (te), and crossover distance (ce) to the uncertainty in h_{N-1} for subsurface models with different velocity structures, where h_{N-1} is the thickness of the layer above the target refractor 50 m from shotpoint A. (a) Box and whisker plots show the interquartile range and range of the outcomes from the MC simulations when each of the error ranges displayed in Table 2 were applied. The model schematics to the right represent the velocity models used to create each of the synthetic datasets and correspond to Fig. 3. (b) Stacked graphs showing the sensitivity indices for h_{N-1} with respect to each of the uncertain inputs for the chosen subsurface models. Subsurface model names correspond to those in Table 1 and Fig. 3.

2. Analysis using synthetic data

2.1. Experiment setup

To explore the interplay between acquisition errors, the complexity of subsurface structure, and the sensitivity of h_i and v_i uncertainty, we created synthetic time-distance (t-x) pairs consistent with a range of velocity-depth models and geophone arrangements (Table 1; Fig. 3). Synthetic raypaths were calculated by honouring Snell's Law at each velocity interface, with ray distance converted to travel-time according to the velocity in each layer.

Gaussian probability distributions were assigned to each of the uncertain input variables (x_D, t_D, and c_i, where D is the geophone number), within the ranges defined in Table 2. Errors in t increase linearly with offset as a way of expressing the reduced signal-to-noise ratio (SNR) associated with attenuation and amplitude decay (Northwood, 1967). For the 'Long Spread' and 'Short Spread' cases, maximum errors in t are updated to 2 ms and 0.5 ms, respectively, to reflect the different maximum offsets.

For the MC simulations, we set $p = 95\%$ and hence m was 200,000. To calculate S_i for x_e, t_e, and c_e, we require $V(X_i)$ for each of these inputs and $V(Y)$ (Eq. 6). Therefore, the MC process was executed five times for each input model, using the error bounds listed in Table 2. The $|r|$ between outputs was <0.005 in all cases, thus justifying the use of the first-order S_i estimate (Taylor, 1990). To make quantitative comparisons between the output thickness and velocity uncertainties, we use the variance, interquartile ranges (IQR), and median values of the resultant pdfs.

The variance values for all of the outputs from the 2-layer tests (Appendix 1a, c, e) show that uncertainty in h_1 is approximately three orders of magnitude greater than that in v_1 or v_2; this is consistent with Hoffmann and Schrott's (2003) observation of larger uncertainties for depth than velocity when using the intercept-time method. Further analysis of the synthetic data therefore focuses on changes in the uncertainty in thickness of the unit above the target refractor, as expressed by the results for the thickness beneath the geophone 50 m offset from shotpoint A (h_{N-1}; dashed lines, Fig. 3).

Fig. 4 shows the spread of output h_{N-1} values for input models with different subsurface structures and survey layouts. Changing the geophone interval or refractor depth has little effect on the output uncertainties and sensitivities, for these and any other reasonable survey geometries, whereas altering the spread length or velocity structure of the subsurface has an observable impact on h_{N-1} uncertainty (Fig. 4). The increase in h_{N-1} uncertainty with spread length is due to deteriorating SNR and hence higher t_e at longer shot-receiver offsets. In both the 2- and 3-layer cases, the estimation of h_{N-1} is most uncertain when the subsurface velocity is high, as is shown by the large IQR for the *3-layer high velocity* and *high velocity* models (Fig. 4). The main influence is the velocity in the unit directly above the target refractor (v_{N-1}) as opposed to the half-space velocity (v_N): the three high-contrast models, in which v_N is high but v_{N-1} is low, produced narrow h_{N-1} IQRs (Fig. 4). Northwood (1967) states that velocity contrast has a large impact on the effect of

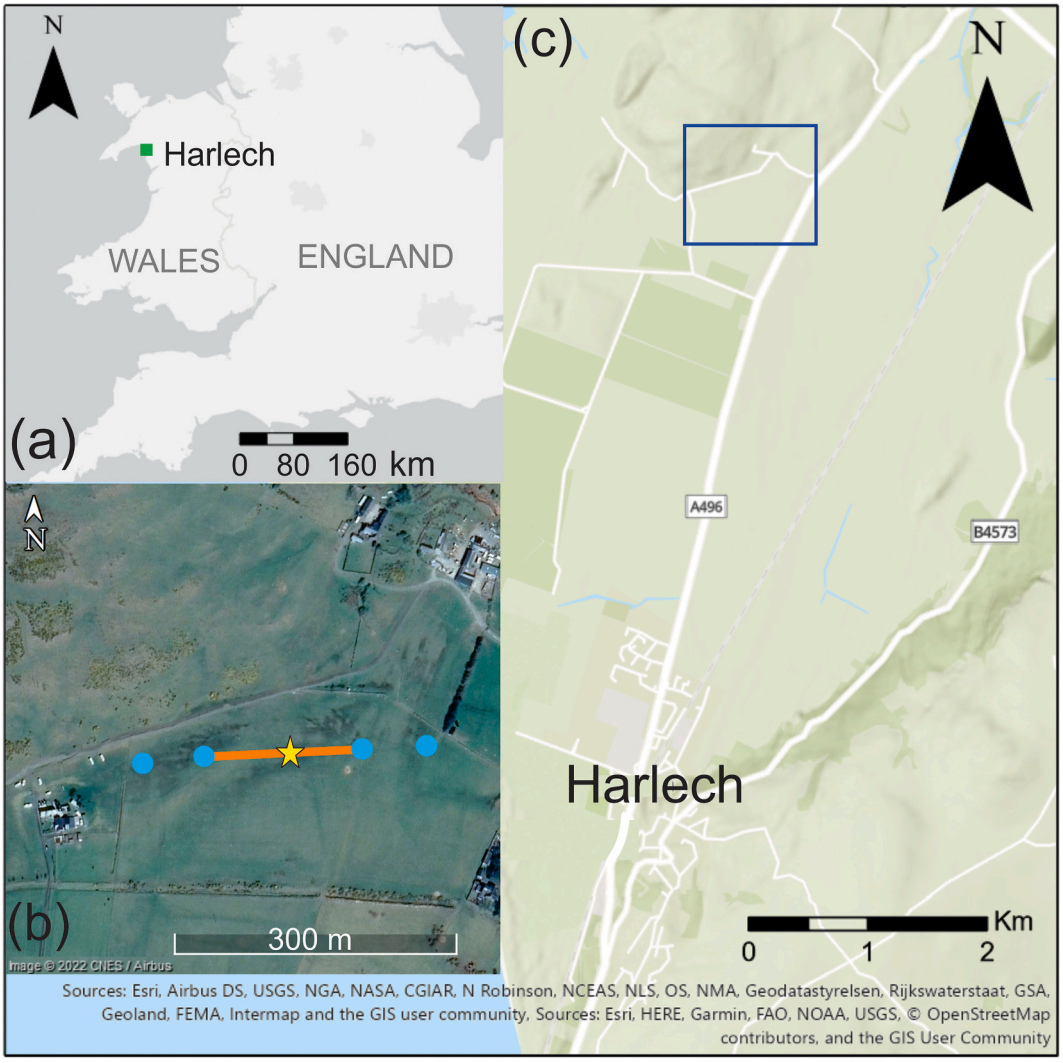

Fig. 6. The location of the field data collection. (a) The green square shows the location of (c) within England and Wales. (b) Satellite image of the field where the survey was carried out (52°53′17" N, 4°06′08" W, yellow star). Orange line shows the position of the seismic survey line and the blue circles the shotpoints. (c) Topographic and street map of the surrounding area with the location of (b) outlined in blue. (For interpretation of the references to colour in this figure legend, the reader is referred to the web version of this article.)

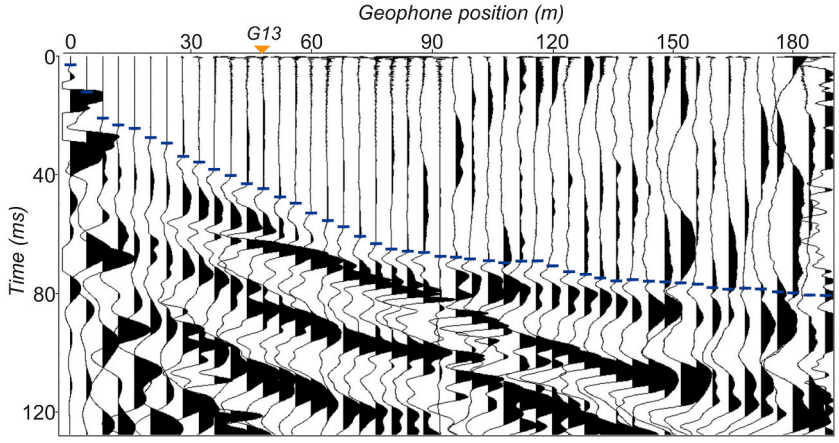

Fig. 7. Shot gather from the shot taken at 0 m offset from geophone 1 at the field site in North Wales. First-break picks for each trace are marked by blue lines. The location of geophone 13 (G13), which is used in our uncertainty analysis, is indicated by an orange triangle. (For interpretation of the references to colour in this figure legend, the reader is referred to the web version of this article.)

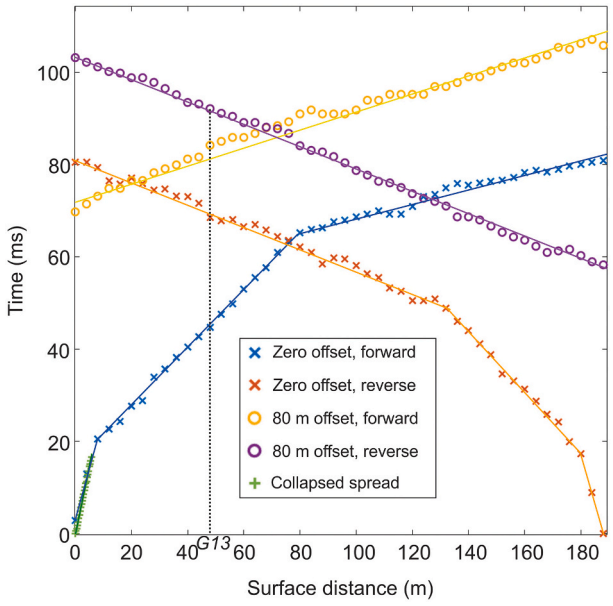

Fig. 8. Time-distance plot of first-break picks from all of the shot gathers from the North Wales field data. Straight lines show the linear segments used in refraction interpretations. The location of geophone 13 (G13) is displayed with a black dotted line. Zero offset and 80 m offset refer to the distance from the shotpoint to the end of the geophone spread and forward and reverse refer to which end the survey was shot from. The Collapsed spread had a smaller geophone spacing and the shot was located at geophone 1.

input uncertainty, with results being particularly sensitive to input uncertainty when the velocity ratio v_{N-1}/v_N is >0.75 (i.e., velocity contrast is low). The results from our 2- and 3-layer high velocity models agree with this, however the '*low contrast*' model ($v_{N-1}/v_N = 0.67$) produced a much narrower IQR than the '*high velocity*' model ($v_{N-1}/v_N = 0.55$) (Fig. 4), supporting our contention that the magnitude of v_{N-1} has a strong influence on h_{N-1} sensitivity to input uncertainty.

The results from the synthetic data tests reveal differences in the contributions from the three input errors, x_e, t_e, and c_e, to the overall output uncertainties (Fig. 5 and A1–2). Fig. 5 shows that h_{N-1} is most sensitive to t_e, except where a high velocity contrast is present. S_i distributions for h_{N-1} are mainly driven by changes in $V(t)$, and variations in $V(x)$ and $V(c)$ are more consistent between the different model outputs. For these simulations, t_e values were assumed to be low, in many field situations, low SNR will reduce the accuracy of first-break picks, meaning the contribution of t_e to output uncertainty will be even more dominant (e.g., Section 3.2). For three-layer cases the sensitivity of h_{N-1} to c_e is more significant than for the two-layer cases, likely due to the inclusion of two crossover locations, however, in all cases, S_c is <0.2 (Figs. 4b and A1–2). Other than the change in S_c, adding an extra overburden layer to the subsurface model has little impact on the uncertainty in h_{N-1} (Figs. 4 and 5).

3. Field data example

3.1. Data collection and processing

Seismic data were collected in flat fields at Ty Cerrig farm, north of Harlech (52°53′17" N, 4°06′08" W; Fig. 6b), Wales, UK. Published geological mapping implies that the site overlies a stratified subsurface of Quaternary glacial material, potentially overlying Tertiary sediments, underlain by southwards-dipping Cambrian bedrock (Allen and Jackson, 1985). The seismic survey deployed 48 geophones at 4 m intervals (a spread length of 188 m), oriented in the assumed strike direction of the bedrock. A PEG-40 accelerated weight-drop (AWD) source was deployed at 0 m and 80 m offset from each end of the spread (zero-offset and 80 m-offset shots, respectively), providing forward and reverse coverage (Fig. 6). To improve the sampling of the direct wave, and thus the constraint on v_1, a collapsed spread was used with 24 geophones at 0.25 m spacing, and a hammer and plate source. All records were 1 s long, with a sampling frequency of 8000 Hz. Up to 22 individual shots were taken at each location and stacked to improve SNR.

Initial processing and manual first-break picking for each of the seismic shot gathers was undertaken in ReflexW (version 8.5.6; Sandmeier, 2016; Fig. 7) and the resultant *t-x* pairs were imported to Matlab (version R2018a; MATLAB, 2018) for analysis with PM. Trigger timing and source impact plate location errors were corrected by applying bulk time shifts to all arrival times, determined from the arrival time of the airwave at a set of reference geophones. PM was applied following Eqs. (1)–(5), for a 3-layer case and dipping layer calculations (Ewing et al., 1939) were used to define the overburden unit thicknesses (h_1) and velocities (v_1 and v_2). v_1 was defined using the collapsed spread *t-x* picks; v_2 and h_1 were calculated using the data from the zero-offset shots; and v_3 and h_2 were defined using the *t-x* picks from the 80 m-offset shots (Fig. 8).

MC simulations were applied to these data using Gaussian probability distributions for each quantity in the PM method, with limits defined by the error bounds in Table 3. Initial error bounds were defined based on the resolution of the inputs, which are determined from the SNR of the seismic data and the field conditions. Although the level field minimised the likely error in geophone placement along a measuring tape, some uncertainty could be introduced by possible deviations of the tape from a straight line and human error when planting the geophones. SNR is high at near offsets, so first breaks are clearly defined, but noise from wind and other ambient noise at further offsets (Fig. 7) reduced the SNR and hence, the accuracy of first-break picks (Table 3). As with the synthetic models, m was 200,000, and using this the entire MC process took just over 1 hour to run on a standard desktop PC.

Table 3
Error bounds used to defined Gaussian probability distributions for the input variables of the field data. Both crossover locations had the same error. First break time errors increase linearly from near to far offset geophones. Full and collapsed spreads used 1 and 4 m geophone separations, respectively. 0 m and 80 m offset refer to the distance from the shotpoint to the end of the geophone spread (Figs. 6, 8).

	Full spread x_e (m)	Collapsed spread x_e (m)	0 m offset t_e (ms)	80 m offset t_e (ms)	Collapsed spread t_e (ms)	c_e (Geophone)
None	0	0	0	0	0	0
Distance	0.5	0.1	0	0	0	0
Time	0	0	1.5–3.0	2.5–4.0	1.5	0
Crossover	0	0	0	0	0	1
All	0.5	0.1	1.5–3.0	2.5–4.0	1.5	1
x: 1	1.0	1.0	0	0	0	0
x: 0.5	0.5	0.5	0	0	0	0
x: 0.05	0.05	0.05	0	0	0	0
t: 10	0	0	10	10	10	0
t: 5	0	0	5	5	5	0
t: 0.5	0	0	0.5	0.5	0.5	0

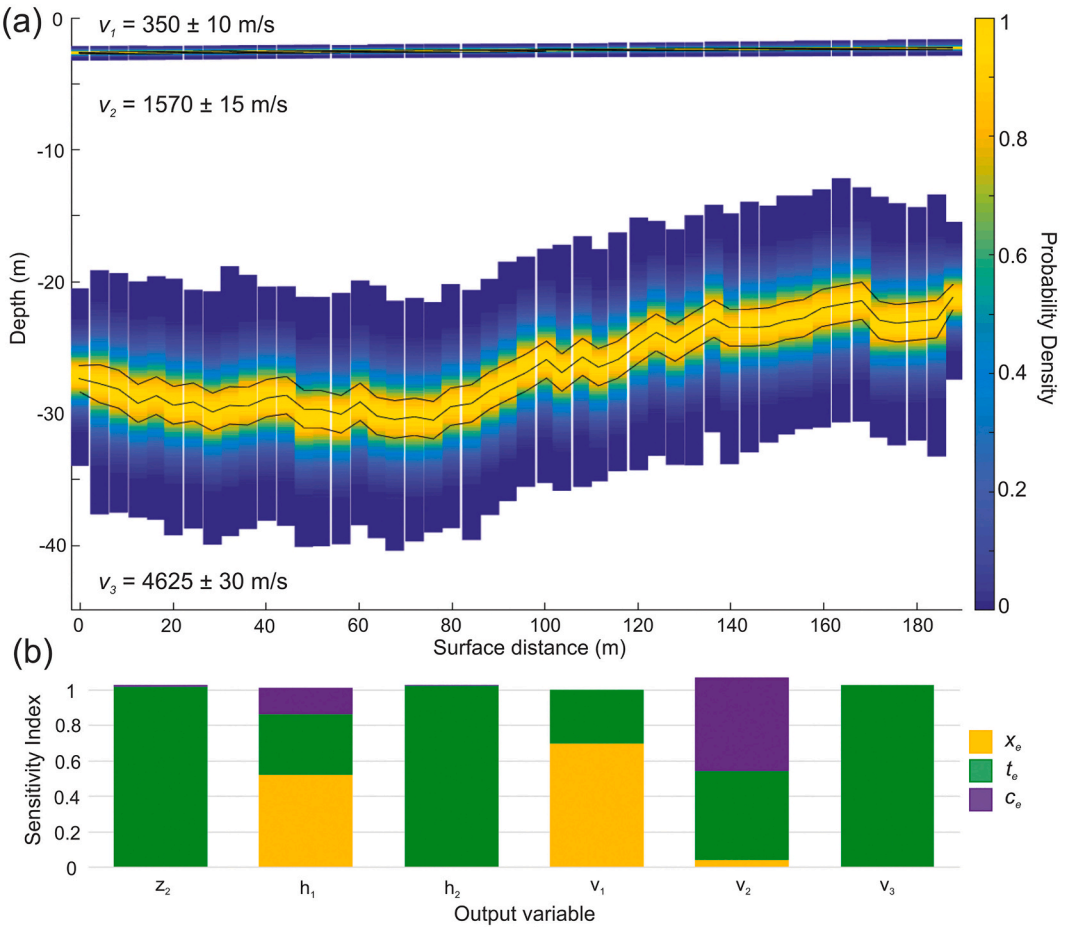

Fig. 9. Results from MC PM analysis of seismic data from North Wales. (a) Modelled refractor surfaces and velocities with uncertainty in depths displayed as probability density functions beneath each geophone location and velocities quoted as the median output values ± half the inter-quartile range. Black lines show the mode, upper and lower quartiles of the depth distributions. The subsurface was modelled assuming 'All' input error bounds (Table 3). (b) Sensitivity indices for output variables with respect to uncertainty in geophone offset (x_e), first-break pick time (t_e), and crossover distance (c_e). z_i, h_i, and v_i are the depth, thickness, and velocity of layer i, respectively.

The output velocity-depth profile, with associated errors, from the MC PM analysis is displayed in Fig. 9. Depths to each boundary are displayed as pdfs at each geophone location, the range of these showing that z_2 uncertainties are greater than those in z_1. This was similarly observed in the *3-layer high velocity* and *3-layer low contrast* synthetic model outputs, which have comparable velocity structures to the Wales site (Appendix 2). Velocity uncertainty also increases with depth, with the IQR in the pdfs increasing from 20 m/s to 60 m/s for v_1 to v_3 respectively. These increases in refractor depth and velocity uncertainties with depth are partly down to the different t_e values assigned to each of the shot gathers (Table 3), but as the synthetic models use just one 'shot gather' to calculate both h_1 and h_2, this must not be the only factor affecting these results, as is further shown is Section 3.2.

The uncertainties in unit velocities and refractor depths propagate through to static correction estimates and hence, through quantifying the uncertainty in h_i and v_i, we can calculate the uncertainty in statics for use in seismic reflection investigations. We applied this analysis to the field data assuming a flat surface topography and calculated the weathering correction at an individual location, i.e., a source or a receiver,

$$T_W = \sum_{i=1}^{n} h_i \left[\frac{1}{v_{w_i}} - \frac{1}{v_e} \right], \tag{7}$$

where n is the number of weathering layers, v_W is the velocity in layer i and v_e is the replacement velocity from below the weathering layer, usually v_{n+1} (Cox, 1999). We applied the static corrections assuming both two-layer ($i = 1$) and three-layer cases ($i = 2$), considering near-surface (e.g. environmental) targets and deep (e.g. resource) targets, respectively. For the two-layer case, $v_e = v_2$ and static corrections are applied to z_1, which was determined using the dipping layer method. For the three-layer case, $v_e = v_3$ and static corrections are applied to z_2, which was determined using PM. It is standard to apply a 'total static' correction to reflection data, which is the sum of the source and receiver statics and as such, we calculated the total static corrections for all possible shot and receiver pairs for each of the model outputs.

The results from the static correction calculations (Fig. 10) demonstrate the significant difference in the magnitude of the uncertainty related to h_1 and h_2. For the total static corrections, when $i = 1$, the interquartile range of the outcomes is 0.3 ms, whereas when $i = 2$, the interquartile range increases to 9.9 ms; this closely to corresponds to the precisions of the refractor depths and is in part due to the larger t_e values associated with the 80 m offset shot gathers. Fig. 11 shows that the input errors introduce a negative bias to T_w, i.e., when refraction results are uncertain, static corrections may leave reflection events at later times, and hence appearing deeper, than is correct.

3.2. Simulated effects of more uncertain data

The flat terrain at our field site was conducive to accurate geophone placement, even without the use of GPS equipment. Furthermore, our surveys used an AWD source, giving high SNR and a confidence in first-

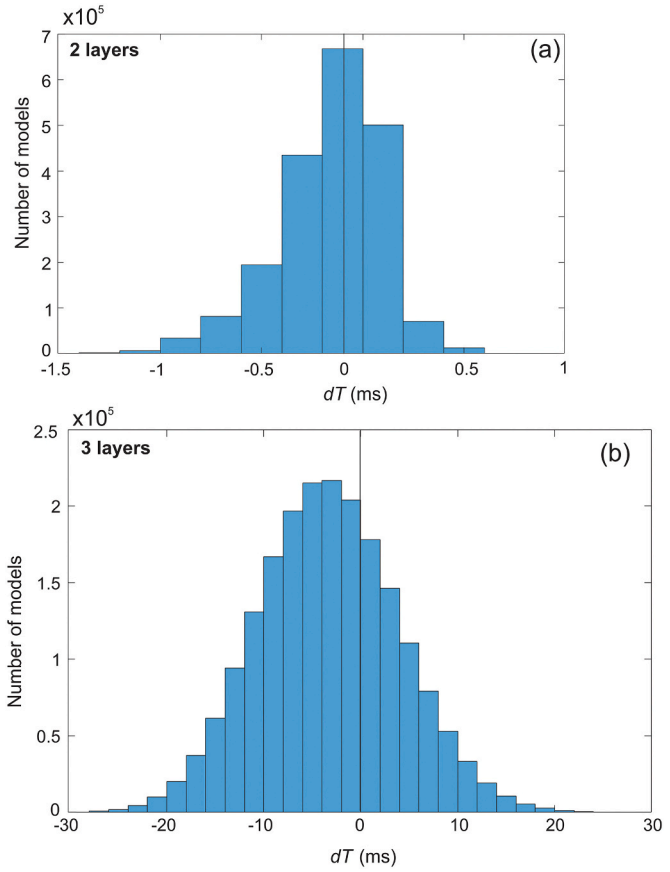

Fig. 10. Static correction uncertainty analysis results. Histograms of all dT values from static calculations assuming two (a) and three (b) layer cases, where dT = Tw_j - Tw_{ref}. Tw_j is the average weathering correction provided by model permutation j and Tw_{ref} is the average weathering correction when it is assumed there is no uncertainty in the refraction interpretation inputs.

break picking at near offsets (±1.5 ms; Table 3). Even at far offsets, where SNR was poorer, first-breaks could still be picked to within ±4 ms. Elsewhere, uneven (e.g., rocky) terrain can impede accurate geophone placement along a prescribed survey line (e.g., Watts et al., 2022), and different sources, weather conditions, or ambient noise can damage SNR and thus the accuracy of first-break picks (Yilmaz, 2001). The impact of these sources of error on h_i uncertainty was explored by imposing different uncertainties on the geophone positions, x_e, and first-break picks, t_e, (Table 3) of our field dataset.

Fig. 11 shows the different uncertainties in refractor depths with cases of i) precise and imprecise geophone positioning, and ii) noise-free and noisy conditions. These outcomes reaffirm our suggestion that t_e has a stronger influence on the uncertainty in z_2 than z_1, and this is not just due to increasing t_e with offset distance, and they show that both depth sensitivities are similar and smaller for x_e. A 10-times increase in either t_e or x_e is amplified tenfold in h_{N-1} variance (Fig. 11e). Proportionally, both input errors have the same effect on the variance of h_{N-1}, showing roughly exponential growth in the uncertainty of h_{N-1} as t_e or x_e increases. However, as the influence of x_e is less than t_e, any plausible error in geophone placement alone is unlikely to be sufficiently large to obscure refractor topography. Where surface obstacles are present (e.g., boulders into which geophones cannot be planted), geophones may be placed out of line: when x_e is set to 1 m, the resultant interquartile range of h_{N-1} is 0.20 m at geophone 13 (48 m from A). Under windy conditions, the additional noise in first-break picks could lead to increased timing uncertainties. Increasing t_e to ±10 ms, the interquartile range of h_{N-1} at the same geophone becomes 8.1 m (Fig. 11d); given that the median value for h_2 changes by a maximum of 5.6 m along the survey line, t_e is sufficiently uncertain to obscure refractor topography. Therefore, it is important that h_i uncertainty is always calculated and stated.

4. Discussion

We have defined an efficient means of evaluating the uncertainty in refractor depths and seismic velocity estimates, calculated using PM. Although PM makes a number of limiting assumptions about the complexity of the subsurface velocity distribution, we anticipate that the sensitivities we report will be directly relevant for more sophisticated analysis methods. The MC PM process could be applied during future seismic studies to (i) calculate and illustrate refractor depths and velocities, along with their associated uncertainty, when the subsurface velocity structure is laterally homogeneous, (ii) provide constraints for inversion starting models, and (iii) determine the uncertainty in geotechnical parameters or static corrections, derived from seismic refraction results.

We have explored in detail the contributions of the three errors, first-break pick times (t_e), shot-geophone offsets (x_e), and crossover distances (c_e) to the uncertainty in refractor depth estimates as these input errors are quantifiable and independent and hence can be evaluated using the MC process. By applying the MC PM process to synthetic data, we have shown that, in most cases, t_e provides the most significant contribution to the overall uncertainty in z_N, of the three errors explored. Since t_e is the most significant source of uncertainty in an output model, field effort should be directed towards maximising SNR - i.e., through the use of more energetic seismic sources and short maximum source-geophone offsets, minimising wind noise on geophones, stacking more sources at any shotpoint, and/or through applying advanced first-break picking techniques (e.g., Zhao et al., 2022). In addition to minimising t_e, efforts should be made to obtain accurate estimates of the magnitude of this error to provide realistic estimates of output uncertainties (e.g., Abakumov et al., 2020).

Here, t_e is defined as the uncertainty in each individual first-break pick introduced by human error and the limited resolution of the data, and as such these errors are independently distributed from geophone to geophone (Liu and Stock, 1993). The correct determination of first-break times is also affected by the distortion of waveforms due to filtering effects (Geldart and Sheriff, 2004; Northwood, 1967) and cycle skipping, where first-breaks are picked a cycle or half cycle too early or, more commonly, late. These are bulk errors and so are not independently distributed, meaning they cannot be represented using MC. Waveform distortion is most commonly caused by frequency filters; these can introduce a precursor half-cycle to the dataset which obscures the true first break. Half-cycle skipping can also occur when the display polarity is interpreted incorrectly and whole-cycle skipping is possible when the SNR is low. As such, data polarity should always be checked and where possible, the risk of distortion should be avoided by only stacking data prior to first-break picking rather than applying frequency filters. The effect of adding half a cycle (12.5 ms) to the layer 2 arrivals from the baseline model (Fig. 3) showed no effect on velocities, since the gradients in the output *t-x* plots are identical, but moved the refractor depth from 9.5 m to 20.3 m depth. This highlights the need for judicious application of frequency filters, and the need to ensure confidence that the correct wavelet phase has been picked.

The lesser and perhaps insignificant affect that uncertainty in geophone placement has on the uncertainty in refractor depths and velocities is of importance for environmental surveys where rugged terrains often preclude optimal geophone placement. Watts et al. (2022) encountered such issues when performing seismic surveys at a glacial foreland in Norway. Geophone planting efforts were impeded by frozen sediments and boulders meaning some geophones were up to 0.3 m laterally offset from the survey line, with poor control on the resultant shot-geophone offset distances. Refraction analysis was applied using the intercept-time technique to provide 1-D velocity-depth profiles, with thickness and velocity uncertainties defined through slope evaluation

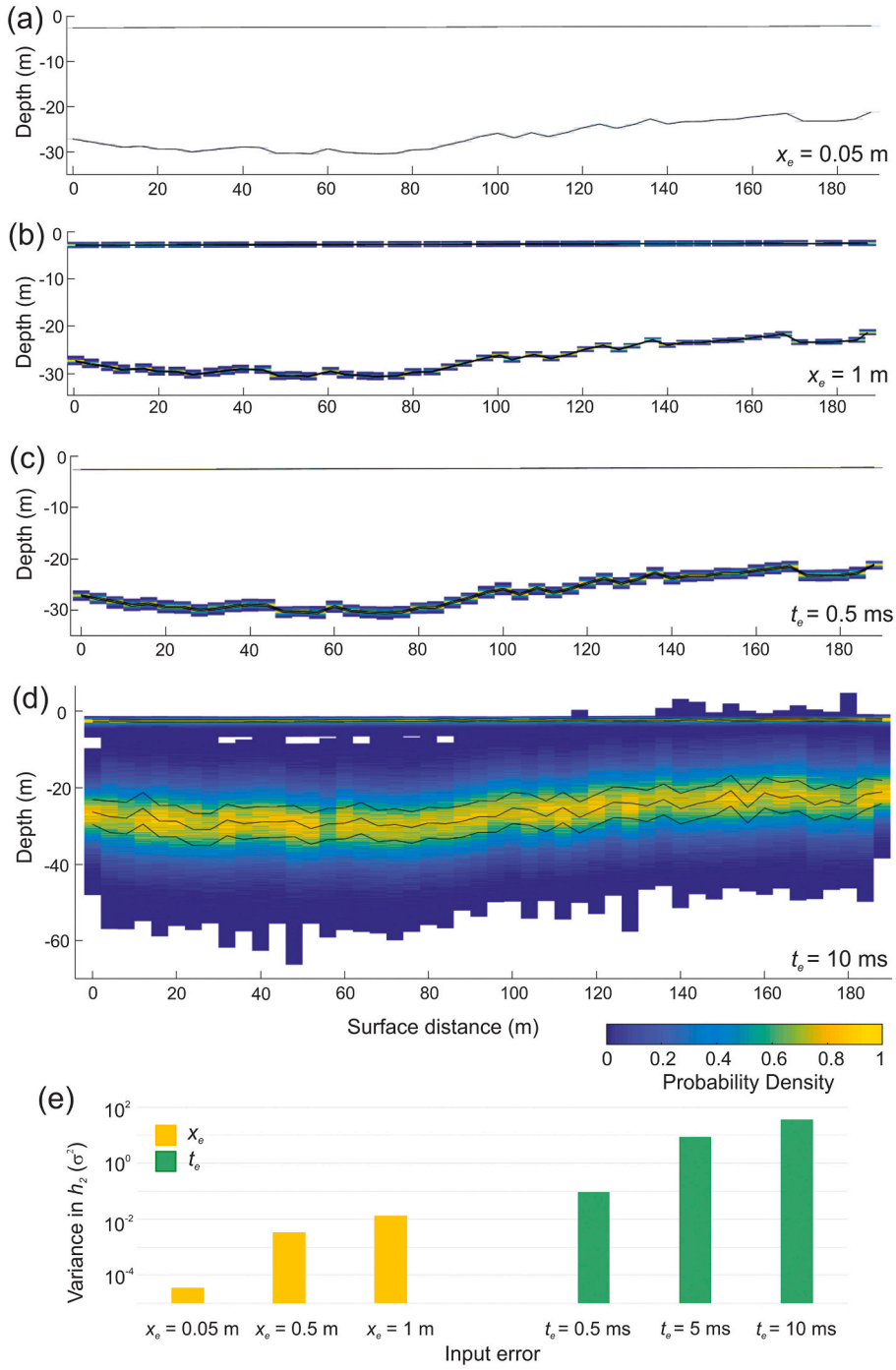

Fig. 11. Results from MC PM analysis of data from North Wales with different input error scenarios. (a–d) Modelled refractor surfaces for different geophone offset uncertainties (a,b) and first-break pick time uncertainties (c,d) with refractor depths displayed as probability density functions with black lines showing the mode, upper and lower quartiles of the output distributions. (e) Variance in modelled thicknesses of layer 2 at geophone 13 (h_2) with different x and t uncertainties.

following the method of York et al. (2004). While this approach considers errors in both *t* and *x*, it does not account for any error interactions which can amplify the overall uncertainty and it does not provide 2-D seismic velocity models. Through applying the MC PM process to the *t-x* picks, depths to the refractive interfaces and associated uncertainties could have been calculated and displayed at each geophone position, rather than as an average for the entire survey line, and changes in t_e and x_e along the survey line could easily be accounted for. Furthermore, the analysis applied here shows that the geophone placement issues will have had little effect on subsurface interpretation. This should reassure any survey team working on rugged terrain, where geophones cannot be placed in line.

The MC PM process successfully represents the uncertainty in seismic velocities and depths to refractive interfaces, considering experimental uncertainties. However, we recognise that we are working at the limits of what PM is capable of and this analysis cannot account for deviations from PM assumptions, such as lateral velocity inhomogeneities, steep surface topography, or local dip effects and there is still a need to define the number of layers, which can be particularly challenging when velocity contrasts are low, there are more than a handful of layers, and dips are anything more than shallow (e.g., Palmer, 1986). Despite this, the values provided can aid subsequent, more advanced, seismic surveys

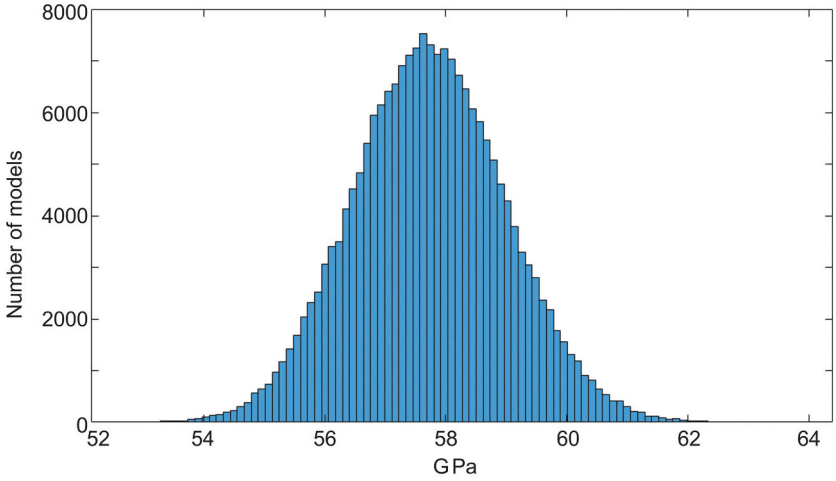

Fig. 12. Results from P-wave modulus (M) calculations. Histogram showing all calculated M values from the MC simulations.

and the calculated P-wave velocities (v_p) can be applied in geotechnical studies to determine parameters such as elastic moduli, porosity, or water content, along with measures of their uncertainty. For example, assuming a normal distribution for density (ρ) based around reported values for Cambrian bedrock, 2700 ± 100 kgm^{-3} (Allen and Jackson, 1985), we calculated the P-wave modulus (M) and its uncertainty for layer 3 at the field site in Wales. Using the v_3 distribution from the MC PM process and the defined ρ distribution, we applied MC simulations to:

$$M = \rho {v_p}^2, \tag{8}$$

to produce a pdf for M (Fig. 12) from which the median and IQR are taken to give $M = 57.7 \pm 0.9$ GPa. M and its uncertainty can then be used along with a shear modulus (G) distribution, obtained from MASW, to define the uncertainty in further geotechnical parameters such as bulk modulus ($K = M - 4G/3$), Young's modulus ($E = G(3M - 4G)/(M - G)$), or Poisson's ratio ($\nu = (M - 2G)/(2M - 2G)$) (Mavko et al., 2009). Defining the ranges of these values is of importance in the field of engineering geology, where such parameters are applied to predict the behaviour of soils and inform construction design.

We have demonstrated here that our fast, and easily implemented, approach to uncertainty definition is beneficial for a wide range of engineering and environmental applications and as such, should be implemented in seismic refraction investigations to provide a first approximation of result uncertainty where state-of-the-art techniques are not financially viable or to optimise the more computing intensive uncertainty definition approaches.

5. Conclusions

Running MC simulations of the PM method is a fast and computationally inexpensive way of propagating input errors to give the uncertainty in output unit velocities and thicknesses. Through applying our MC PM process, the resultant uncertainty in the depth to a refractive boundary can easily be displayed. As such, we would recommend the application of this method to: (i) provide constrained estimates of subsurface velocities and unit boundary depths for environmental studies, when a laterally uniform subsurface is present; (ii) determine static corrections and their associated uncertainty for seismic reflection surveys; (iii) assess the uncertainty in geotechnical parameters, derived from seismic velocities; (iv) constrain starting models for tomographic inversions or MASW.

In most near-surface surveying situations, the impact of errors in geophone placement on target refractor depth uncertainty is apparently minimal compared to the contribution of first-break pick time errors, and this is especially prevalent when a high velocity overburden is present. As such, reliable refraction results can be produced when the surface terrain impedes accurate geophone placement, but the accuracy of first-break picks must be maximised and reliably defined to present representative and informed interpretations.

Funding

This work was supported by the Bolin Centre for Climate Research [2020] and Carl Mannerfelts foundation [2019].

CRediT authorship contribution statement

Hannah Watts: Conceptualization, Methodology, Formal analysis, Investigation, Data curation, Writing – original draft, Visualization. **Adam D. Booth:** Conceptualization, Methodology, Writing – review & editing, Supervision. **Roger A. Clark:** Methodology, Formal analysis, Resources, Writing – review & editing, Supervision. **Benedict T.I. Reinardy:** Writing – review & editing, Supervision.

Declaration of Competing Interest

The authors declare that the research was conducted in the absence of any commercial or financial relationships that could be construed as a potential conflict of interest.

Data availability

The field data and Matlab code used in and created for this analysis can be found on Figshare at: https://doi.org/10.6084/m9.figshare.c.6035696

Acknowledgements

Field data was collected by students on the University of Leeds' MSc Exploration Geophysics course. The Morgan family permitted access to sites at Ty Cerrig farm. Dr. Mark Thomas provided information on the parameters used in Engineering Geology. Valuable comments were provided by two anonymous reviewers.

Appendix A. Appendices

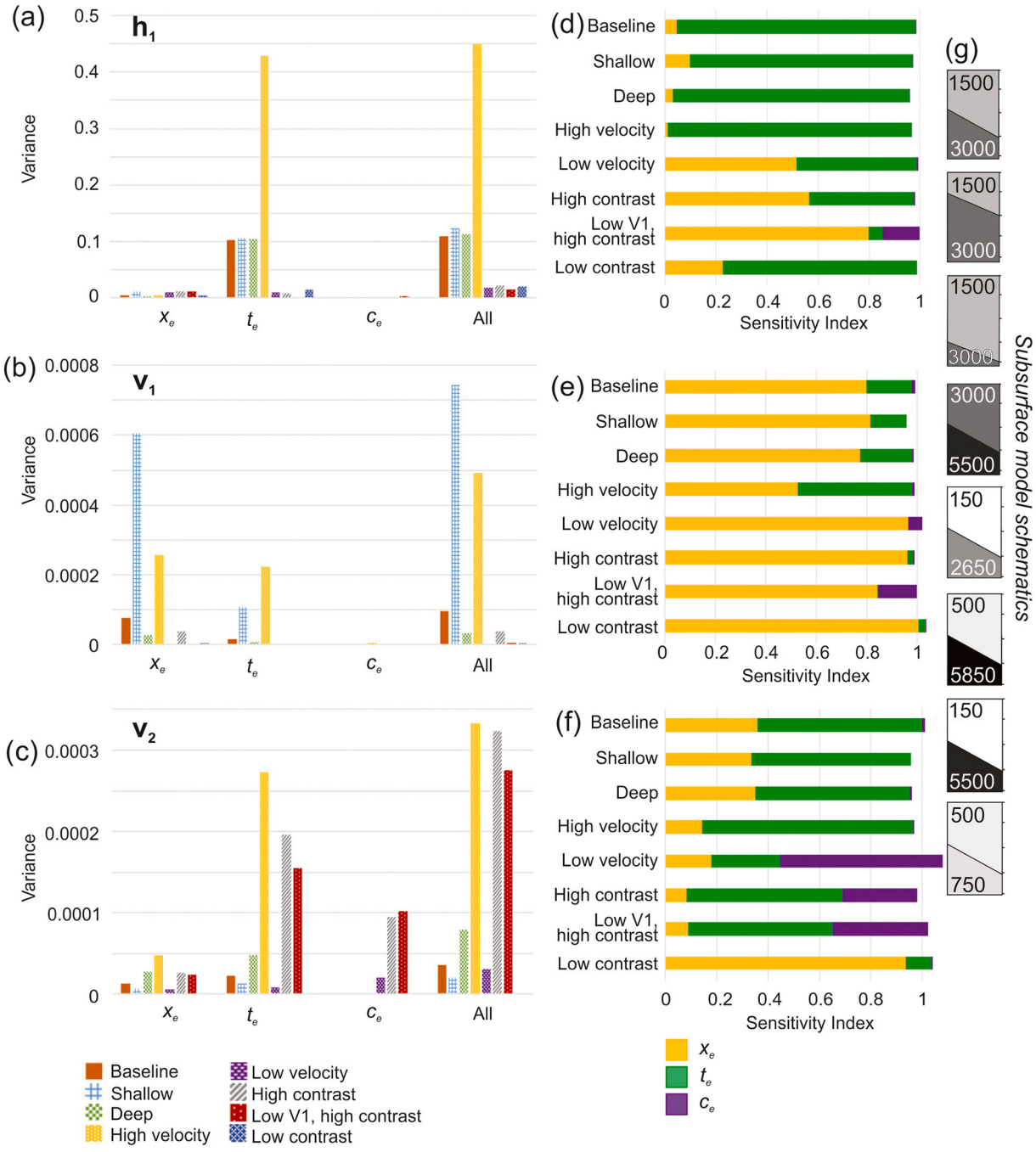

Appendix 1. Results from uncertainty analysis of all 2-layer synthetic datasets. (a–c) Variance in thickness (h_1) and velocity (v_1 and v_2) outputs from MC PM analysis with uncertain geophone offset (x_e), first-break pick time (t_e), and crossover distance (c_e) inputs. (d–f) Sensitivity indices for h_1, v_1, and v_2, respectively, for each of the synthetic datasets. (g) Schematics of the synthetic model velocity structures; order corresponds to the model order in (d) to (f). Model names correspond to Table 2.

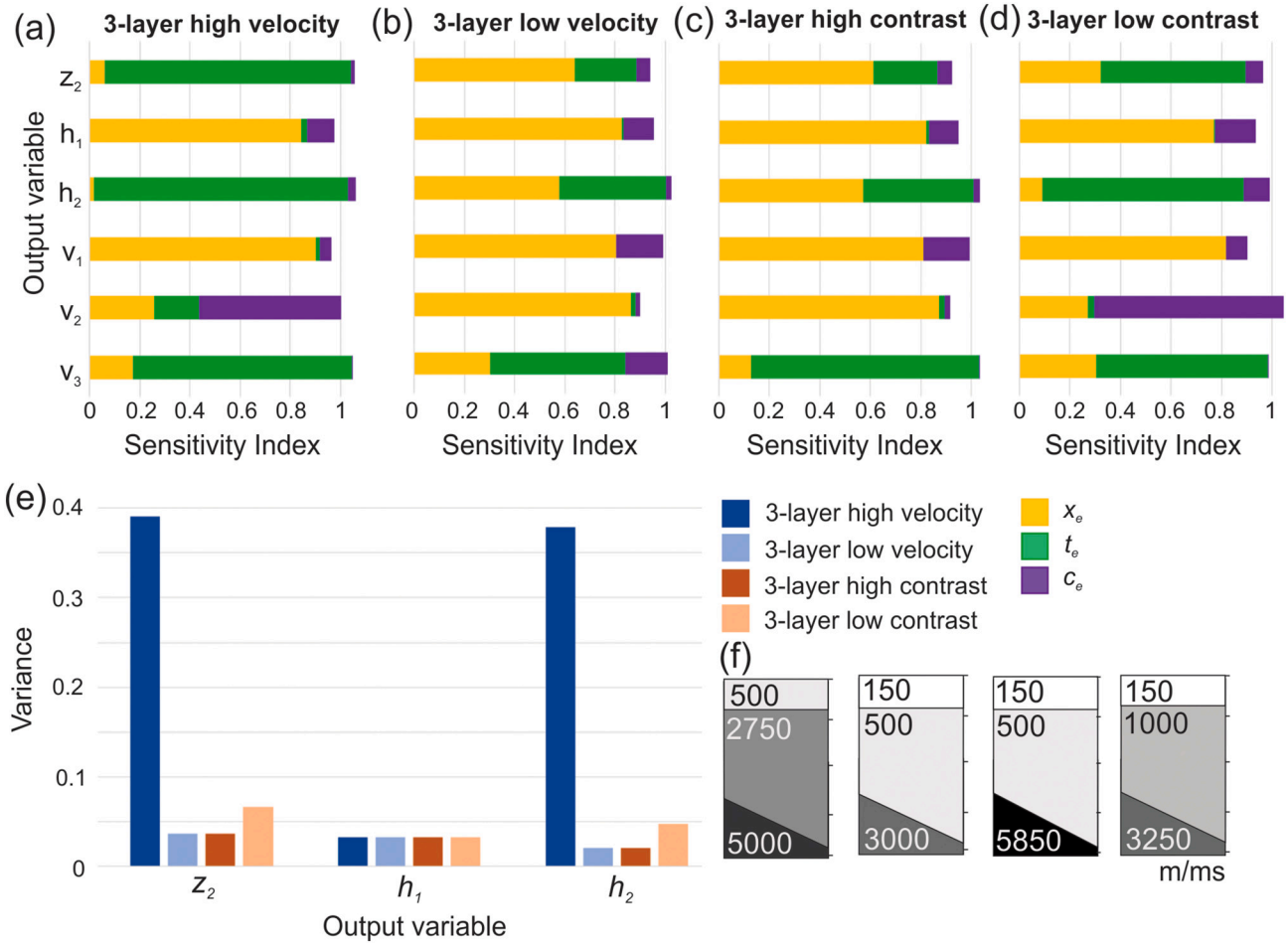

Appendix 2. Results from uncertainty analysis of all 3-layer synthetic datasets. (a–d) Sensitivity indices for the output variables from the four synthetic models depicted in (f). (e) Variance in depth (z_2) and thickness (h_1 and h_2) estimates when 'All' input uncertainties were applied (Table 2).

References

Abakumov, I., Roeser, A., Shapiro, S.A., 2020. Arrival-time picking uncertainty: Theoretical estimations and their application to microseismic data. Geophysics 85, U65–U76. https://doi.org/10.1190/GEO2019-0589.1.

Allen, P.M., Jackson, A.A., 1985. Geology of the country around Harlech. In: Memoir for 1:50 000 Geological Sheet 135 with Part of Sheet 149, (England and Wales). H.M. Stationery Office, London.

Anderson, G.M., 1976. Error propagation by the Monte Carlo method in geochemical calculations. Geochim. Cosmochim. Acta 40, 1533–1538. https://doi.org/10.1016/0016-7037(76)90092-2.

Berry, M.J., 1971. Depth uncertainties from seismic first-arrival refraction studies. J. Geophys. Res. 76, 6464–6468. https://doi.org/10.1029/jb076i026p06464.

Beven, K., 2018. Environmental modelling: an uncertain future?, 1st ed, Environmental Modelling: an Uncertain Future? CRC Press, London. https://doi.org/10.1201/9781482288575.

Booth, A.D., Mercer, A., Clark, R., Murray, T., Jansson, P., Axtell, C., 2013. A comparison of seismic and radar methods to establish the thickness and density of glacier snow cover. Ann. Glaciol. 54, 73–82. https://doi.org/10.3189/2013AOG64A044.

Bridle, R., 2007. Plus-minus method to solve large-amplitude near-surface static corrections. Near Surf. Geophys. 5, 321–330. https://doi.org/10.3997/1873-0604.2007013/CITE/REFWORKS.

Casella, G., George, E.I., 1992. Explaining the gibbs sampler. Am. Stat. 46, 167–174. https://doi.org/10.1080/00031305.1992.10475878.

Couto, P., Damasceno, J., Pinheiro de Oliveira, S., 2013. Monte Carlo Simulations Applied to Uncertainty in Measurement. In: Chan, V. (Ed.), Theory and Applications of Monte Carlo Simulations. InTech, pp. 27–51. https://doi.org/10.5772/53014.

Cox, M., 1999. Static Corrections for Seismic Reflection surveys. In: Society of Exploration Geophysicists, Tulsa, Oklahoma. https://doi.org/10.1190/1.9781560801818.

Cox, M.G., Siebert, B.R.L., 2006. The use of a Monte Carlo method for evaluating uncertainty and expanded uncertainty. Metrologia 43, S178–S188. https://doi.org/10.1088/0026-1394/43/4/s03.

Dampney, C.N.G., Whiteley, R.J., 1980. Velocity determination and error analysis for the seismic refraction method. Geophys. Prospect. 28, 1–17. https://doi.org/10.1111/j.1365-2478.1980.tb01207.x.

Egorov, A., Silvestrov, I., Bakulin, A., 2022. Effect of Vertical Arrays on Near-Surface Velocity and Statics uncertainty. 83rd EAGE Annu. Conf. Exhib. 2022, 1–5. https://doi.org/10.3997/2214-4609.202210103.

Ewing, M., Woollard, G.P., Vine, A.C., 1939. Geophysical investigations in the emerged and submerged Atlantic Coastal Plain: Part III: Barnegat Bay, New Jersey, section. Bull. Geol. Soc. Am. 50, 257–296. https://doi.org/10.1130/GSAB-50-257.

Gardner, L.W., 1939. An areal plan of mapping subsurface structure by refraction shooting. Geophysics 4, 247–259. https://doi.org/10.1190/1.1440501.

Gardner, L.W., 1967. Refraction seismograph profile interpretation. In: Musgrave, A.W. (Ed.), Seismic Refraction Prospecting. Soc. Expl. Geophys Tulsa, Okla, pp. 338–347.

Geldart, L.P., Sheriff, R.E., 2004. Problems in Exploration Seismology and their Solutions. In: Society of Exploration Geophysicists, Tulsa, Oklahoma. https://doi.org/10.1190/1.9781560801733.

Hagedoorn, J.G., 1959. The plus-minus method of interpreting seismic refraction sections. Geophys. Prospect. 7, 158–182. https://doi.org/10.1111/j.1365-2478.1959.tb01460.x.

Hamby, D.M., 1994. A review of techniques for parameter sensitivity analysis of environmental models. Environ. Monit. Assess. 32, 135–154. https://doi.org/10.1007/BF00547132.

Hammersley, J.M., Handscomb, D.C., 1964. Monte Carlo Methods. Chapman and Hall, London. https://doi.org/10.1007/978-94-009-5819-7.

Hausmann, H., Krainer, K., Brückl, E., Mostler, W., 2007. Internal structure and ice content of Reichenkar rock glacier (Stubai Alps, Austria) assessed by geophysical investigations. Permafr. Periglac. Process. 18, 351–367. https://doi.org/10.1002/ppp.601.

Hawkins, L.V., 1961. The reciprocal method of routine shallow seismic refraction investigations. Geophysics 26, 806–819. https://doi.org/10.1190/1.1438961.

Hoffmann, T., Schrott, L., 2003. Determing sediment thickness of talus slopes and valley fill deposits using seismic refraction - a comparision of 2D interpretation tools. In: Zeitschrift Für Geomorphologie. Borntraeger, Berlin, pp. 71–87.

Huang, M.H., Hudson-Rasmussen, B., Burdick, S., Lekic, V., Nelson, M.D., Fauria, K.E., Schmerr, N., 2021. Bayesian Seismic Refraction Inversion for critical Zone Science

and Near-Surface applications. Geochem. Geophys. Geosyst. 22, e2020GC009172 https://doi.org/10.1029/2020GC009172.
Liu, C., Stock, J.M., 1993. Quantitative determination of uncertainties in seismic refraction prospecting. Geophysics 58, 553–563. https://doi.org/10.1190/1.1443438.
MATLAB, 2018. Version 9.4.0.813654 (R2018a). The MathsWorks Inc., Natick, Massachusetts.
Mavko, G., Mukerji, T., Dvorkin, J., 2009. Seismic wave propagation. In: The Rock Physics Handbook. Cambridge University Press, pp. 81–168. https://doi.org/10.1017/CBO9780511626753.004.
Mollaret, C., Wagner, F.M., Hilbich, C., Scapozza, C., Hauck, C., 2020. Petrophysical Joint Inversion Applied to Alpine Permafrost Field Sites to image Subsurface Ice, Water, Air, and Rock Contents. Front. Earth Sci. 8, 85. https://doi.org/10.3389/FEART.2020.00085/BIBTEX.
Morgan, M., Henrion, M., 1990. The Propagation and Analysis of uncertainty. In: Henrion, Max, Morgan, M.G. (Eds.), Uncertainty: A Guide to Dealing with Uncertainty in Quantitative Risk and Policy Analysis. Cambridge University Press, Cambridge, pp. 172–219. https://doi.org/10.1017/CBO9780511840609.009.
Northwood, E.J., 1967. 9. Errors in refraction interpretation. Gen. Ser 458–466. https://doi.org/10.1190/1.9781560802679.CH5E.
Opara, C., Adizua, O.F., Ebeniro, J., 2018. Application of Statics Correction in the Processing of 3D Seismic Data from Onshore Niger Delta. Univers. J. Geosci. 6, 1–7. https://doi.org/10.13189/ujg.2018.060101.
van Overmeeren, R.A., 2001. Hagedoorn's plus-minus method: the beauty of simplicity. Geophys. Prospect. 49, 687–696. https://doi.org/10.1111/j.1365-2478.1964.tb01888.x.
Palmer, D., 1980. The Generalized Reciprocal Method of Seismic Refraction Interpretation. Society of Exploration Geophysicists, Tulsa. https://doi.org/10.1190/1.9781560802426.
Palmer, D., 1981. An introduction to the generalized reciprocal method of seismic refraction interpretation. Geophysics 46, 1508–1518. https://doi.org/10.1190/1.1441157.
Palmer, D., 1986. Refraction seismics: The lateral resolution of structure and seismic velocity. In: Helbig, K., Treitel, S. (Eds.), Handbook of Geophysical Exploration, vol. 13. Geophysical Press, London, p. 269.
Pegah, E., Liu, H., 2016. Application of near-surface seismic refraction tomography and multichannel analysis of surface waves for geotechnical site characterizations: a case study. Eng. Geol. 208, 100–113. https://doi.org/10.1016/j.enggeo.2016.04.021.
Pegah, E., Liu, H., 2020. Evaluation of hyperbolic stress-strain and bulk-modulus model parameters in granular soil mass using seismic surveying. Eng. Geol. 266, 105456 https://doi.org/10.1016/J.ENGGEO.2019.105456.
Razavi, S., Gupta, H.V., 2015. What do we mean by sensitivity analysis? The need for comprehensive characterization of "global" sensitivity in Earth and Environmental systems models. Water Resour. Res. 51, 3070–3092. https://doi.org/10.1002/2014WR016527.
Reynolds, J.M., 2011. An Introduction to Applied and Environmental Geophysics, 2nd ed. Wiley-Blackwell, Chichester, UK.
Rockwell, D.W., Schenck, F.L., Musgrave, A.W., Woolley, W.C., Gray, H., 1967. 8. Wavefront Methods. Gen. Ser, pp. 362–457. https://doi.org/10.1190/1.9781560802679.CH5D.
Ross, N., Brabham, P., Harris, C., 2019. The glacial origins of relict "pingos", Wales, UK. Ann. Glaciol. 60, 138–150. https://doi.org/10.1017/aog.2019.40.
Rossi, G., Accaino, F., Boaga, J., Petronio, L., Romeo, R., Wheeler, W., 2018. Seismic survey on an open pingo system in Adventdalen Valley, Spitsbergen, Svalbard. Near Surf. Geophys. 16, 89–103. https://doi.org/10.3997/1873-0604.2017037.
Ryberg, T., Haberland, C., 2018. Bayesian inversion of refraction seismic traveltime data. Geophys. J. Int. 212, 1645–1656. https://doi.org/10.1093/GJI/GGX500.
Saltelli, A., Tarantola, S., Campolongo, F., Ratto, M., 2004. Sensitivity Analysis in Practice : A Guide to Assessing Scientific Models. John Wiley & Sons, Ltd, Ispra, Italy.
Sandmeier, K.J., 2016. GPR and Seismic Data Processing Software - Sandmeier [WWW Document]. URL. https://www.sandmeier-geo.de/.
Schuster, G.T., Quintus-Bosz, A., 1993. Wavepath eikonal traveltime inversion: theory. Geophysics 58, 1314–1323. https://doi.org/10.1190/1.1443514.
Sobol', I.M., 1993. Sensitivity estimates for nonlinear mathematical models. MMCE 1, 407–414.
Tarantola, A., 1986. A strategy for nonlinear elastic inversion of seismic reflection data. Geophysics 51, 1893–1903. https://doi.org/10.1190/1.1442046.
Taylor, R., 1990. Interpretation of the Correlation Coefficient: a Basic Review. J. Diagnostic Med. Sonogr. 6, 35–39. https://doi.org/10.1177/875647939000600106.
Thornburgh, H.R., 1930. Wave-Front Diagrams in Seismic Interpretation. Am. Assoc. Pet. Geol. Bull. 14, 185–200. https://doi.org/10.1306/3d9328ad-16b1-11d7-8645000102c1865d.
Virieux, J., Operto, S., 2009. An overview of full-waveform inversion in exploration geophysics. Geophysics 74, WCC1–WCC26. https://doi.org/10.1190/1.3238367.
Watts, H., Booth, A.D., Reinardy, B.T.I., Killingbeck, S.F., Jansson, P., Clark, R.A., Chandler, B.M.P., Nesje, A., 2022. An assessment of geophysical survey techniques for characterising the subsurface around glacier margins, and recommendations for future applications. Front. Earth Sci. 10, 298. https://doi.org/10.3389/FEART.2022.734682/BIBTEX.
Whiteley, R.J., 2004. Shallow seismic refraction interpretation with visual interactive ray trace (VIRT) modelling. Explor. Geophys. 35, 116–123. https://doi.org/10.1071/EG04116.
Whiteley, R.J., Eccleston, P.J., 2006. Exploration Geophysics Comparison of shallow seismic refraction interpretation methods for regolith mapping Comparison of shallow seismic refraction interpretation methods for regolith mapping. Explor. Geophys. 37, 340–347. https://doi.org/10.1071/EG06340.
Ye, M., Hill, M.C., 2017. Global sensitivity analysis for uncertain parameters, models, and scenarios. In: Sensitivity Analysis in Earth Observation Modelling. Elsevier Inc., pp. 177–210. https://doi.org/10.1016/B978-0-12-803011-0.00010-0
Yilmaz, Ö., 2001. Seismic Data Processing and Seismic Data Analysis, 2nd ed. Society of Exploration Geophysicists, Tulsa.
York, D., Evensen, N.M., López Martínezmartínez, M., De, J., Delgado, B., 2004. Unified equations for the slope, intercept, and standard errors of the best straight line. Cit. Am. J. Phys. 72, 367. https://doi.org/10.1119/1.1632486.
Zhang, K., Lu, Z., Cheng, L., Xu, F., 2015. A new framework of variance based global sensitivity analysis for models with correlated inputs. Struct. Saf. 55, 1–9. https://doi.org/10.1016/j.strusafe.2014.12.005.
Zhao, T., Bilsby, P., Manikani, S., Busanello, G., Benzaoui, M., Abubakar, A., 2022. Deep Learning Ensemble for Seismic First-Break Event Picking. 83rd EAGE Annu. Conf. Exhib, 2022, pp. 1–5. https://doi.org/10.3997/2214-4609.202210425.
Zhu, X., Gao, R., Li, Q., Guan, Y., Lu, Z., Wang, H., 2014. Static corrections methods in the processing of deep reflection seismic data. J. Earth Sci. 2014 252 (25), 299–308. https://doi.org/10.1007/S12583-014-0422-X.